J. Math. Biol. (2017) 74:981–1009
DOI 10.1007/s00285-016-1045-x

Mathematical Biology

Geometric indicators of population persistence in branching continuous-space networks

Jonathan Sarhad[1] · **Scott Manifold**[2] · **Kurt E. Anderson**[1]

Received: 21 July 2015 / Revised: 11 May 2016 / Published online: 20 August 2016

Abstract We study population persistence in branching tree networks emulating systems such as river basins, cave systems, organisms on vegetation surfaces, and vascular networks. Population dynamics are modeled using a reaction–diffusion–advection equation on a metric graph which provides a continuous, spatially explicit model of network habitat. A metric graph, in contrast to a standard graph, allows for population dynamics to occur within edges rather than just at graph vertices, subsequently adding a significant level of realism. Within this framework, we stochastically generate branching tree networks with a variety of geometric features and explore the effects of network geometry on the persistence of a population which advects toward a lethal outflow boundary. We identify a metric (CM), the distance from the lethal outflow point at which half of the habitable volume of the network lies upstream of, as a promising indicator of population persistence. This metric outperforms other metrics such as the maximum and minimum distances from the lethal outflow to an upstream boundary and the total habitable volume of the network. The strength of CM as a predictor of persistence suggests that it is a proper "system length" for the

This work was supported by a National Science Foundation Grant No. DMS-1122726 to J. Sarhad and K.E. Anderson and a University of California, Riverside Chancellor's Research Fellowship to S. Manifold.

✉ Kurt E. Anderson
kurt.anderson@ucr.edu

Jonathan Sarhad
jonathan.sarhad@gmail.com

Scott Manifold
scott.manifold@u.northwestern.edu

[1] Department of Biology, University of California, Riverside, CA 92521, USA

[2] Department of Engineering Science and Applied Mathematics, Northwestern University, Evanston, IL, USA

branching networks we examine here that generalizes the concept of habitat length in the classical linear space models.

Keywords Population dynamics · Branching networks · Reaction–diffusion–advection · Partial differential equations · (Metric) graph theory · Principal eigenvalue analysis

Mathematics Subject Classification 05C12 (distance in graphs) · 35K57 (reaction–diffusion) · 58C40 (spectral theory; eigenvalue problems) · 35K20 (initial-boundary value problems for second-order parabolic equations) · 35J25 (boundary value problems for second-order elliptic equations) · 92D40 (ecology)

1 Introduction

Many natural phenomena are studied using graph theory. A major area of inquiry is how graph structure influences dynamics on the graph. Researchers have identified numerous geometric indicators which appear to partially explain dynamics on graphs (e.g., Strogatz 2001; Albert and Barabasi 2002; Barrat et al. 2008). However, the overwhelming majority of studies have focused on the structure and dynamics associated to standard graphs, which, in their simplest form, consist of collections of vertices ("objects," "nodes," "patches,") and edges ("branches," "links," "connections,") which link some pairs of vertices. While many applications exploit these edge relations for additional structure, for example, using edge weights and directions, the edges themselves are rarely considered part of a spatial domain where dynamics occur.

In contrast, many biological systems such as river basins, cave systems, organisms on vegetation surfaces, and vascular networks have a spatial structure which may be more appropriately modeled by metric graphs, which allow for dynamics to occur within edges (e.g., Ramirez 2012; Sarhad et al. 2014; Sarhad and Anderson 2015). Unlike standard graphs, metric graphs encode spatially continuous networks where edges represent actual habitat rather than merely connections among discrete nodes. Dynamic equations are defined edgewise with edgewise dynamics then "glued" together by junction conditions. This mathematical formalism is often referred to as *quantum graphs* (Berkolaiko and Kuchment 2012; also see citations in Sarhad et al. 2014).

Quantum graph theory has great potential for informing how branching network structure influences the dynamics of biological systems, a topic that has attracted extensive theoretical and empirical attention (Altermatt 2013; Brown et al. 2011; Fausch et al. 2002; Grant et al. 2007; Reynolds and Cuddington 2012). Recent advances in methodology and statistics have improved our ability to represent and analyze data in the context of branching networks such as rivers (e.g. Peterson and Hoef 2010; Peterson et al. 2013). However, a unified body of theory that can explain and predict emerging patterns is lacking. Most previous studies have either considered dynamics on a line, representing individual reaches or branches (e.g., Anderson et al. 2005; Lutscher et al. 2005; Speirs and Gurney 2001) or artificially discretizing an essentially continuous system to a set of interconnected patches (e.g., Auerbach and Poff 2011; Fagan 2002;

Goldberg et al. 2010; Muneepeerakul et al. 2007). These previous studies have shown that dispersal constrained to limited reaches of habitat and/or by network configuration can influence persistence of populations inhabiting the network domain. Yet, while these approaches have been fruitful in isolating certain aspects of network geometry and their effects on ecological outcomes, they possess limitations. The linear approach limits the scope of results to small spatial scales while the potential shortcomings of discrete patch representations of continuous space call for alternative methods which present continuous space networks in a more natural way (Brown et al. 2011; Grant et al. 2007).

1.1 Aims and outline

While the application of the quantum graph framework to biological problems is in its beginning stages, it holds great promise for representing realistic continuous spatial variability in habitat size and quality, dispersal characteristics, and other environmental and demographic parameters that cannot be represented using discrete patch models. Previous studies (Sarhad et al. 2014; Sarhad and Anderson 2015) have identified geometric indicators of population persistence in highly symmetric networks which can be described using relatively few parameters. However, actual networks such as rivers or vegetation branches are decidedly not symmetric and can differ greatly in size and shape. It is unclear how limited insights from previous studies transfer to contexts with more complex geometries, as geometric indicators relating dynamics to geometry in metric graphs are generally lacking. The foremost aim of the current article is to isolate the effects of geometry on population persistence by identifying metrics encoding global geometry that are capable of predicting persistence outcomes. Due to the mathematical complexity and number of geometric parameters incorporated in a quantum graph model, including novel effects brought about by behavior at junctions (Sarhad et al. 2014), it is still prudent to introduce a number of simplifications. We therefore ignore within-edge variability as well as assume that dispersal and population growth parameters are uniform over the entire network. It is our aim to acquire a strong basic understanding of the effect of network geometry on persistence that can be applied to more complex and system-specific models.

Under the simplifications described above, we challenge the ability of metrics to describe population persistence in stochastically generated networks that vary in topology and the distribution of habitable area. Section 3 presents results from two case studies that impose alternative conditions on relative habitat sizes around a junction. We define Case 1 in a manner that is consistent with the interpretation of hydrologic conservation of discharge at junctions in river networks, should a species' advection speed coincide with river flow and its habitat comprise the full volume of the network. Case 2 is more general, allowing for the same flexibility in a species' advection characteristics, while also allowing for a broad range of species-dependent habitable spaces within the network. While Case 1 allows for—but is not limited to—a strictly hydrological interpretation, we consider advection speed decoupled from flow and habitable space decoupled from actual physical space such as vessel size or wetted perimeter in both Cases 1 and 2. The motivation for this, in the context of advection, is that it

affords the freedom to represent a bias in direction of a population as the net result of any environmental forces and species-dependent behavioral characteristics which may affect the directed component of dispersal. Similarly, a more realistic measure of habitat is assumed, as most species' habitable space is strictly less than that afforded by branch or channel size and can be affected by a species' characteristics as well as environmental conditions. While our modeling efforts are initially motivated by river networks, the assumptions made above aim for generality such that our results can be applied to a wide range of biological systems.

Our results numerically compare the performance of various metrics. One such metric, CM, emerges as the strongest predictor of persistence by our numerical analysis. Further analysis demonstrates that this metric is a proper generalization of the concept of "system length" in population persistence studies to the branching networks we consider here. As our primary focus is to isolate the effects of habitat geometry on persistence, our initial studies use a single fixed combination of dispersal parameters. However, to verify the robustness of our initial results, we include additional Case 1 and Case 2 studies that feature a broad range of dispersal values; CM continues to outperform the other metrics in these cases. While measures such as CM have a long history in hydrology and geomorphology (Rodriguez-Iturbe and Rinaldo 2001), to our knowledge they have not been previously identified as an indicator of population persistence in branching networks.

Since the mathematics used here are fairly technical, we refer readers to previous work and the Appendix for many of the more technical aspects in order to reach a wide audience. The Appendix (Sect. 5) features a brief description of the mathematics involved (Sect. 5.1) that includes a concrete example and computation (Sect. 5.3). The Appendix also features two stochastic studies which provide additional evidence of robustness of the CM metric as well as offering further intuition into the nature of the persistence problem in quantum graphs (Sect. 5.2).

2 Model and methods

2.1 Population model

The fundamental component of our on-network population model is a single-species reaction–diffusion–advection (RDA) equation

$$\frac{\partial u_e}{\partial t} = D_e \frac{\partial^2 u_e}{\partial x_e^2} - V_e \frac{\partial u_e}{\partial x_e} + F_e(u_e) \tag{2.1}$$

which describes the spatial population dynamics in a network segment e (Speirs and Gurney 2001; Cantrell and Cosner 2003). For the current article we consider e as a finite interval. The state variable $u_e(t, x_e)$ is population density (volume) at time t and position x_e in the segment e such as a river reach or a tree branch. Population dispersal is a combination of diffusion and a directional bias in transport (advection). The diffusion coefficient $D_e > 0$ approximates the scale of random (Brownian) movement in the segment e, intended to model a composite of redistribution due to turbulence,

swimming, crawling or other forms of undirected movement. The advection speed in the segment e, $V_e \geq 0$, adds a directed component to population dispersal such as drift which, in river systems, can differ from current speed due to organism behavior. The population reaction term, F_e, encodes birth and death processes.

2.2 Persistence criteria

Population persistence is characterized by population growth in the linearized model

$$\underbrace{\frac{\partial u_e}{\partial t} = D_e \frac{\partial^2 u_e}{\partial x_e^2} - V_e \frac{\partial u_e}{\partial x_e} + r_e u_e, \quad r_e = \frac{\partial F_e}{\partial u_e}(0)}_{\text{linearization of } F_e \text{ around } 0} \tag{2.2}$$

Persistence occurs if (and only if) a small population u_e, with *intrinsic growth rate* $r_e > 0$, can grow asymptotically in time.

In the current article, we consider only finite habitats and impose boundary conditions at habitat boundaries. Specifically, we adhere to commonly used boundary conditions: the zero flux condition (organisms do not enter or leave the habitat) at an upstream boundary b and the lethal condition (organisms die or washout of the habitat of interest) at a downstream boundary a (Speirs and Gurney 2001; Lutscher et al. 2005):

$$\underbrace{u_e(t,a) = 0}_{\text{lethal}} \qquad \underbrace{D\frac{\partial u_e}{\partial x_e}(t,b) = V u_e(t,b)}_{\text{zero flux}} \tag{2.3}$$

Via a typical separation of time and space variables, the linearized RDA (2.2), augmented with boundary conditions on a segment e, leads to the following spatial eigenvalue equation:

$$D\frac{\partial^2 U_e}{\partial x_e^2} - V\frac{\partial U_e}{\partial x_e} + r_e U_e = \lambda U_e \tag{2.4}$$

where $U_e = U_e(x_e)$ (see Appendix, Sect. 5.1, for details) and the boundary conditions are unchanged except for the omission of the time variable t. A substitution $\Lambda = r_e - \lambda$ is useful in studying persistence analysis, in which case Λ is the eigenvalue for the diffusion-advection operator

$$-D\frac{\partial^2 U_e}{\partial x_e^2} + V\frac{\partial U_e}{\partial x_e} = \Lambda U_e \tag{2.5}$$

This eigenvalue problem features a principal (smallest) eigenvalue Λ_1 (of an infinite number of Λ_k for $k = 1, 2, 3\ldots$) which depends on the dispersal parameters (V and D), segment length L, and the boundary conditions, while the term $\lambda = r_e - \Lambda_1$ determines whether the population governed by (2.2) grows or shrinks to zero as $t \to \infty$ (see, e.g., Cantrell and Cosner 2003; Lutscher et al. 2005; Sarhad et al. 2014; Speirs and Gurney 2001). Indeed, since Λ_1 is smallest of the Λ_k and hence λ is the largest (dominant) of the $r_e - \Lambda_k$, the persistence criteria then becomes

$$\lambda = r_e - \Lambda_1 > 0 \longleftrightarrow \text{Population Persistence in a Segment} \tag{2.6}$$

For this reason, we refer to Λ_1 as the obstruction the intrinsic growth rate r_e must overcome in order to assure persistence. The quantity λ which determines asymptotic growth or decay in (2.2) is analogous to the dominant eigenvalue commonly featured in other population persistence analyses (e.g., integro-differential models, matrix models, etc). Since Λ_1 is independent of r_e and therefore better isolates the effects of habitat geometry on persistence, Λ_1 is the focus of our investigation. Given homogenous coefficients, the computation of Λ_1 is routine for a bounded segment by finding the smallest positive root of the determinant of a 2×2 matrix.

2.3 Extension to networks

The network models introduced in Sarhad et al. (2014), Sarhad and Anderson (2015) and used here extend the case of the finite segment with boundary conditions to continuous tree networks. The extended model features boundary conditions as well as junction conditions (Fig. 1b–d) which we address in further detail below. We naturally consider tree-shaped networks here which branch upward from a root vertex toward upstream boundaries (Fig. 1c). Extending the RDA to a continuous tree requires the identification of the tree with a metric tree graph where each segment (or edge) e is

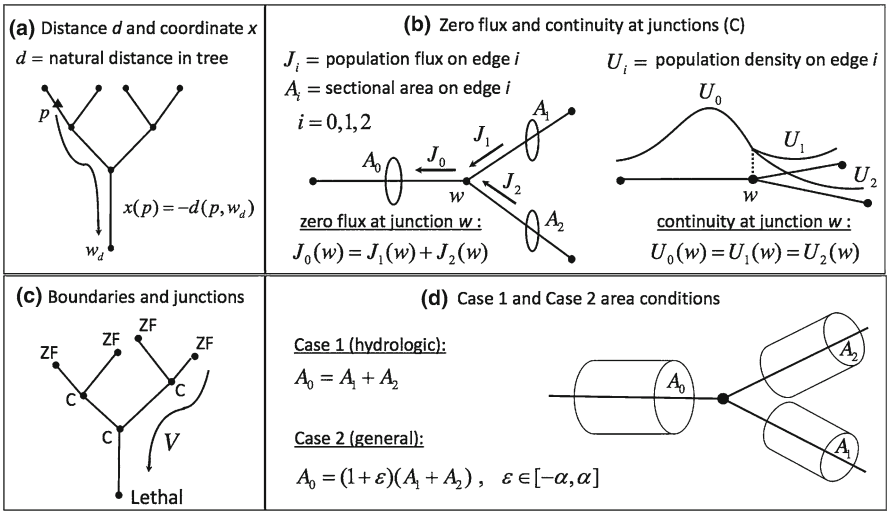

Fig. 1 Schematic for quantum tree graphs: **a** illustrates distance in a metric tree graph and a function x which provides a coordinate for any point in a tree. **b** Illustrates the habitable sectional areas A assigned to each edge and the zero flux condition at a junction. **c** Example of a continuous function on the tree at a junction. **b** and **c** Together provide an example of the zero flux and continuity condition (C) we impose at junctions in all of our models. **d** Provides the area conditions that are assumed for each of our two cases studies. Case 1 is consistent with, although not limited to, the interpretation of hydrologic conservation of discharge at junctions in river networks; Case 2 is more general. In both cases we assume habitable space is decoupled from actual physical space

identified with a real line interval $[a, b]$. The lengths of these intervals may differ from edge to edge. This identification produces a natural metric or distance function d on the graph (Fig. 1a) in the obvious way: one considers all of the (continuous) paths from a point p to a point q in the tree, and their corresponding distances are given by the lengths of the intervals (and sub-intervals) associated with the (partial) edges the paths traverse. The minimum of these is defined as the distance.

In the current article, we consider rooted binary tree graphs with root vertex denoted w_d. The function $x(p) = -d(p, w_d)$ increases toward zero at the root vertex (Fig. 1a). The function x induces local edge-wise coordinates. Subsequently, the RDA is defined explicitly on each segment of the tree. A given edge is assigned an edgewise coordinate, denoted x_e, which is the address of a point p in edge e at a given distance from the root.

Any vertex with exactly one incident edge is referred to as a boundary point (Fig. 1c). In the tree network, an interior vertex has three incident edges and is referred to as a junction (Fig. 1). The RDA process on the tree is the result of the individual processes on each of the edges whose interactions are mediated by junction conditions and boundary conditions. A useful convention for labeling the three edges (and corresponding edge-related data, including function values) incident on an arbitrary junction uses the subscripts $i = 0, 1, 2$, where 0 denotes the edge closest to the root vertex (Fig. 1b). This "local" notation around a junction is useful in describing junction conditions and understanding their affects on persistence, however, the mathematics requires a global addressing system $e = 1, 2, \ldots, m$, for a tree with m edges. There is no unique addressing system, so any discussion of a global addressing system is omitted from the remainder of the article.

As mentioned in the introduction, it is assumed that V, D, and r are uniform over the network so that the subscript e can be dropped from these parameters; that is, organisms diffuse, advect, and reproduce at the same rate everywhere in the tree. We chose this simplified dispersal mechanism with only two dispersal parameters (V and D) since it aids in isolating how the geometric features of a tree-like habitat affect persistence. Our networks feature varying lengths L_e and habitable sectional areas A_e which are assigned to each tree segment e (Fig. 1b). The habitable space available within each segment is idealized by an insulated cylindrical pipe (with cross sectional area A) that runs along the segment (Fig. 1d). Since the areas approximate habitable space, they are decoupled from the actual physical cross section of the network segment. As advection is also decoupled from hydrologic flow speed or other physical processes, our model is not restricted to a conservation of hydrologic discharge at junctions ($A_0V = A_1V + A_2V$) though this can be considered as a special case.

2.4 Persistence criteria in networks

The eigenvalue problem (2.5) takes the exact same form in our tree networks as on each segment of the tree, with the principal eigenvalue Λ_1 being edge-independent. The Eq. (2.5) is defined on each segment of the tree and then "glued" together by a "zero flux plus continuity" junction conditions (C) (Fig. 1b). Upstream boundary

conditions maintain zero flux (ZF) and the lethal condition holds at the root of the tree. The zero flux part of condition C at junctions is precisely the condition that organisms cannot enter or leave the habitat (the tree network) at a junction (the flux *into* $(J_1 + J_2)$ a junction w must equal the flux *out of* (J_0) a junction w; see Fig. 1b). The continuity part of condition C maintains the population (volume) densities on each of the three incident edges to a junction are equal at the junction. Condition C, at an arbitrary junction w, is given by

$$\underbrace{A_0\left(VU - D\frac{\partial U_0}{\partial x_0}\right)(w) = A_1\left(VU - D\frac{\partial U_1}{\partial x_1}\right)(w) + A_2\left(VU - D\frac{\partial U_2}{\partial x_2}\right)(w)}_{\text{zero flux: } J_0(w)=J_1(w)+J_2(w)} \tag{2.7}$$

$$\underbrace{U(w){:=}U_0(w) = U_1(w) = U_2(w)}_{\text{continuity}} \tag{2.8}$$

The persistence criteria for the tree network has exactly the same form as (2.6),

$$\lambda = r - \Lambda_1 > 0 \iff \text{Population Persistence in a Network} \tag{2.9}$$

however, Λ_1 is now dependent on many geometric parameters (every segment length L_e and cross sectional area A_e of the network) in contrast to a single segment length. An additional departure from the single segment model which is featured in networks is that Λ_1 is influenced by the interaction of geometric parameters and dispersal parameters at a junction (see (2.7); see also Sarhad et al. 2014; Sarhad and Anderson 2015). The computation of Λ_1 in bounded networks is less trivial than in the single segment case but, analogously, Λ_1 is numerically calculated as smallest positive root of the determinant of a $2n \times 2n$ matrix, for a network with n edges. We refer to the Appendix (see Sects. 5.1 and 5.3) for further details on computing Λ_1 in networks. Note that from (2.7), it is immediately apparent that Λ_1 does not depend on a uniform rescaling of all habitable areas of the network but does depend on the ratios A_1/A_0 and A_2/A_0 at each junction as these ratios affect junction behavior. This is a significant departure from the single segment model, where Λ_1 is independent of habitable cross-sectional area.

We note that there are mathematical requirements that ensure that principal eigenvalue of analysis of the linearized Eq. (2.2) are meaningful in the context of population persistence; these are discussed in more detail in the Appendix, Sect. 5.1.

2.5 Network-related metrics as indicators of persistence

Isolating a relatively simple metric that is able to predict the behavior of the principal eigenvalue over a wide range of river networks would minimize the effort of computing persistence outcomes and at the same time provide conceptual insight on how habitat geometry affects persistence. The primary focus of the current article is to develop and test the robustness of global geometric features of river networks as indicators of

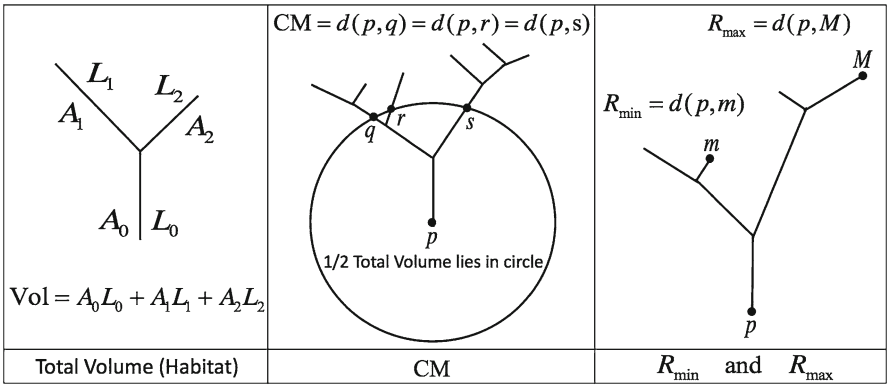

Fig. 2 Persistence metrics used in this study. Each of the four geometric features of branching networks featured in our studies are pictured above. The *left side* features an example computation of the total volume of the network. The *middle figure* is an example of the median of the volumetric width function CM which is a gauge of how the network volume is distributed relative to the network root. The *right side* provides examples of the distances R_{max} and R_{min} which are the distances to the root, respectively, from the farthest and closest upstream boundaries

persistence (Fig. 2). Here, a "global metric" assigns a real number to a network that is meant to quantify aspects of the network's geometry, preferably those aspects most crucial to persistence. Some of these, like the total volume of the network Vol, R_{min} (distance from downstream root to nearest upstream boundary) and R_{max} (distance from downstream root to farthest upstream boundary), have appeared in the context of the persistence problem in Sarhad et al. (2014) as bounds for principal eigenvalues and in numerical studies of radial trees.

While Vol depends on all of the areas and lengths assigned to the network, it is blind to the location of the network boundaries, and in particular, the lethal root. In contrast, R_{min} and R_{max} encode distance to the lethal root but nothing about habitat volume, ignoring cross sectional areas completely. In the limited numerical studies of radial trees in Sarhad et al. (2014), these three metrics are shown to be relevant to varying degrees, depending on the study. Yet, it is the *distribution of volume* that emerges as a consistently important factor in determining persistence across all studies in Sarhad et al. (2014). The volume distribution concept is the inspiration for our final metric we refer to as the Center Metric, or CM, which is the radius from the root (i.e. lethal outflow) that encapsulates half of the network volume. This metric is the median of the volumetric width function often used to characterize geometry in hydrological and geomorphological studies (Rodriguez-Iturbe and Rinaldo 2001).

The volume of a network Γ is simply the sum of the volumes of all of the edges of Γ. An edge e has volume A_eL_e (see the picture in Fig. 1d) so that the volume of Γ, Vol(Γ), is given by

$$\text{Vol}(\Gamma) = \sum_{e \in \Gamma} A_e L_e \tag{2.10}$$

See Fig. 2 (left) for an example. CM, in general, is not easily written in analytic form but is readily obtained numerically. The same is true of R_{min} and R_{max}, examples of which

are shown in Fig. 2 (right). Although CM is designed to encode habitat distribution with respect to the lethal boundary, it is also influenced by the ratios A_1/A_0 and A_2/A_0, and subsequently encodes some information about junction behavior in the system.

2.6 Network structure and simulations

In order to test the robustness of metrics described above as indicators of persistence, we stochastically generate metric graph networks and subsequently analyze the resulting distribution of principal eigenvalues with respect to each of indicator. The networks are all rooted binary trees, meaning that all internal vertices have three incident edges. The root edge possesses one branching vertex and one terminal vertex; terminal vertices are those with no further branching. Therefore, *with the exception of this root vertex (and therefore the root edge)*, the topologies of the graphs are those of full (but not perfect) rooted binary trees, being connected to either zero or two other vertices (with the "root" of such a tree being the neighbor of our actual root vertex). Our simulations here only consider trees with 14 vertices (i.e., 13 edges), yet, because we are employing metric graphs, each network possesses additional geometric structure beyond the traditional topology of a standard graph. This includes edge lengths and areas whose values are also determined stochastically, which is discussed in more detail below. Example trees are presented in (Fig. 3).

Networks are generated using the following algorithm. First, two vertices are connected to the branching vertex of the root edge. Connections among vertices are then

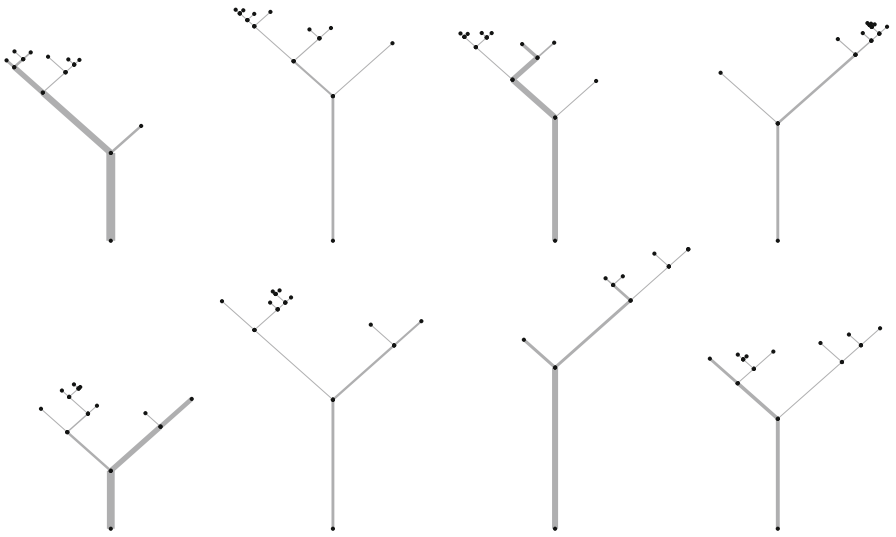

Fig. 3 Example networks used in this study. Each network is a metric tree graph generated using the algorithm described in the text. *Dots* (•) represent vertices that are associated with either junction or boundary conditions while *lines* (—) represent edges. The thickness of the lines in the figure are proportional to the cross-sectional area A associated with the edge. Networks shown above are generated using Case 1 area conditions (2.11) although Case 2 networks exhibit similar topologies

recursively constructed where, at each step, a vertex is randomly chosen as available to bifurcate until the number of vertices reaches the desired number (here 14). Next, edge lengths are generated, starting with the root edge length L_1 that is chosen from a uniform distribution $[a, b]$. Subsequent edge lengths are chosen from a uniform distribution $[a_n, b_n]$ at each level of the tree n increasing from the root edge at $n = 1$. The length of $[a_n, b_n]$ is half of the length of the previous distribution $[a_{n-1}, b_{n-1}]$ such that

$$L_n \approx \frac{1}{2} L_{n-1} = \cdots = \left(\frac{1}{2}\right)^{n-1} L_1$$

Therefore, second level lengths are chosen from $[a/2, b/2]$, third level lengths are chosen from $[a/4, b/4]$, and so on. Our choice of exponential scaling recapitulates basic natural patterns such as those found in river drainages (Rodriguez-Iturbe and Rinaldo 2001) and plant vessel networks (Bentley et al. 2013), with a value of 1/2 used for simplicity and generality. For river drainages, our selection implies that all branching levels are of a given Horton order (Rodriguez-Iturbe and Rinaldo 2001), although this does not account for side tributaries of smaller order common in real rivers. Our scaling value also falls within the range observed for tree vessel branching networks (Bentley et al. 2013).

The distributions used to assign habitable areas are partitioned into two cases. These cases include different cross sectional area conditions assumed around junctions (Fig. 1d). Case 1 is consistent with the interpretation that advection speed is the flow speed of a river or fluid in a vessel network and the cross sectional areas represent the actual river channel or vessel sizes. This condition holds the sum of the cross sections in each level of the tree as constant. This can be represented as follows

$$A_0 = A_1 + A_2 \tag{2.11}$$

where, in accordance with our local addressing system at an arbitrary junction, A_0 represents the cross section of the edge directly downstream of the junction, while A_1 and A_2 represent the cross sections of the edges directly upstream of a junction. Condition (2.11) is consistent with hydrologic conservation of discharge ($A_0 V = A_1 V + A_2 V$). However, we note that this is not a necessary interpretation, since the habitable areas around a junction may all be smaller than their corresponding channel sizes, yet still satisfy $A_0 = A_1 + A_2$. In addition, the advection speed V may differ from flow and yet it still holds that $A_0 V = A_1 V + A_2 V$. Case 1 is used in Sect. 3.1.

The Case 2 condition (Fig. 1d) is more general, decoupling advection speed from the flow speed (interpreting advection as a directional bias in movement in the downstream direction) and habitable areas from channel or vessel size, allowing for a departure from hydrological conservation of discharge. In particular, we are interested in an ε neighborhood of the equality condition in (2.11), which is represented as follows

$$A_0 = (1 + \varepsilon)(A_1 + A_2), \quad \varepsilon \in [-\alpha, \alpha] \tag{2.12}$$

While we studied a range of different α values, for simplicity we hold $\alpha = 0.5$ for Case 2 studies in Sects. 3.2 and 3.4.

To differentiate from the "local" subscripts on areas, we denote the root edge area by A_r, which like L_1, is chosen from a uniform distribution $[a, b]$. For Case 1, an adjacent upstream edge area is chosen from the uniform distribution $(0, A_r)$ while the other adjacent edge area is obligated to satisfy (2.11), a pattern which continues up the tree. Similarly, for Case 2, an adjacent upstream edge area is chosen from $(0, A_r/(1+\varepsilon))$, while the other adjacent edge area is obligated to satisfy (2.12), and so on.

For both the Case 1 and Case 2 studies in Sect. 3, L_1 is chosen from [0.5, 1.5] and A_r is chosen from [0.5, 2]. However, Sect. 5.2 of the Appendix features studies on both larger and smaller root edge length and area distributions. Section 5.2 studies illustrate robustness of the metric CM to changes in the root edge length and area distributions.

Since our focus in the current article is on branching network geometry, we begin with a simplified case where $V = D = 1$ is held constant. With this parameter set, we generate 1000 trees each for Cases 1 and 2. To test that our initial results stand up to variation in dispersal, we include studies where persistence metrics are tested across a range of V and D value for 100 generated trees. For all studies, we maintain zero-flux (ZF) upstream boundary conditions and a lethal condition at the downstream root boundary, with continuity (C) at all junction conditions (Fig. 1d).

It is important to note that accurate and exhaustive simulation of any particular ecological or biological network is not the goal of this project, as the specifics of these are themselves a subject of wide-ranging inquiry (Rodriguez-Iturbe and Rinaldo 2001; Bentley et al. 2013; Zanardo et al. 2013). Our networks, with 13 edges, already has 26 geometric parameters (13 edge lengths and 13 sectional areas), with the relative positions (volume distribution) of these geometric parameters in the network also of crucial importance (see Sarhad et al. 2014). Thus, the trees used in this article exhibit a wide range of geometries and edge characteristics for testing the robustness of persistence indicators. By selecting a simple and yet geometrically broad framework for studying these effects, we aim to provide a step towards understanding the interplay between persistence and network geometry in more system-specific contexts.

In order to quantify the strength of relationship between principal eigenvalues and each metric, we fit quadratic regressions and compute the resulting R^2 values. If a ΔAIC value suggests a quadratic function overfits the relationship relative to a linear one, the simpler linear function and its corresponding R^2 value is used. We use $\Delta\text{AIC} < 2$ as a cutoff for a quadratic versus linear fit.

3 Investigation and results

3.1 Case 1

Figure 4 shows a monotonic decreasing relationship as well as overall variation of the principal eigenvalue Λ_1 with each of the four metrics. The negative dependence confirms intuition and previous results that increasing the length or volume of a domain

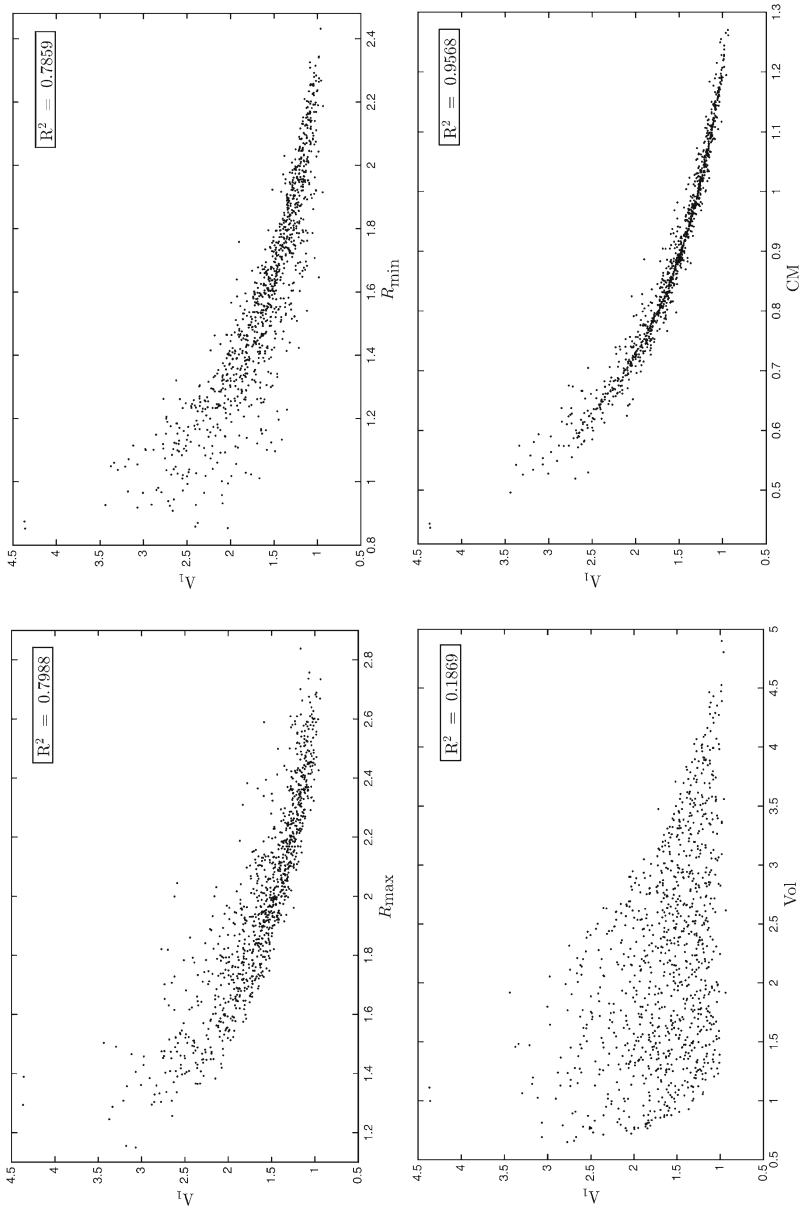

Fig. 4 Persistence metrics for Case 1. Each of the four plots features the given persistence metric versus the principal eigenvalue for 1000 stochastically generated river networks [under Case 1 area conditions: (2.11)]. The dispersal parameters are held constant at $V = D = 1$. CM far outperforms the other metrics both from visual inspection and in terms of the R^2 measure of the point clouds

decreases the principal eigenvalue and hence enhances persistence. The relationship between total volume (Vol) and the principal eigenvalue Λ_1 is weak relative to the other metrics, suggesting Vol is a poor persistence indicator. This agrees with more focused analytic and numerical results in Sarhad et al. (2014) and empirical results from Anderson et al. (2006) that habitat size alone cannot adequately characterize population persistence in a system. While $R_{\min}$ and $R_{\max}$ seem promising in characterizing the behavior of Λ_1, it is CM that best predicts both qualitatively and quantitatively the principal eigenvalue.

We note that the association between all metrics and Λ_1 is weakest when the metric value is relatively small. Heuristically, a small metric value corresponds to a "small" network (measured in terms of any of the four metrics) in which case stochastic perturbations to geometry have disproportionate effects on persistence, increasing variance in outcomes.

3.2 Case 2

With the relaxation of the Case 1 junction conditions, the relationship between three of the four metrics and Λ_1 weakens (Fig. 5). However, the relative ranking of each of the metrics from Case 1 is maintained, with CM far outperforming Vol, R_{max}, and R_{min}. Both $R_{\max}$ and $R_{\min}$ weaken greatly as indicators of persistence in comparison with CM; the latter performs nearly the same as in Case 1 (Fig. 4). A particular point of interest the behavior of the total volume Vol. In contrast with the other metrics, Vol improves slightly from Case 1 to Case 2 despite still being the weakest indicator. This result is likely due to the ability of Vol to capture what we interpret as "congestion" at junctions that can occur when Case 1 area relations do not hold. This congestion appears to occur when the downstream sectional area is smaller than the sum of the two upstream sectional areas, leading to a strong population differential at the junction in the direct of advection (see Sarhad et al. 2014 for an in-depth exploration of this phenomenon). As with Case 1, the Case 2 results show that all metrics suffer the most when their values are relatively small.

3.3 Variation in advection and diffusion

For Case 1, the four metrics are essentially unaffected by the variation in V and D and CM maintains its superiority over the other three metrics as a persistence predictor (Fig. 6). This pattern generally holds under the more general Case 2 area conditions, yet here all metrics suffer drastically under the large values of V/D (Fig. 7). CM performs as well in Case 2 as in Case 1 for all but the most extreme values of V/D and again consistently outperforms the other metrics. On the other hand, $R_{\max}$ and $R_{\min}$ suffer significantly as V/D becomes larger. The metric Vol, which is still the worst predictor over most combinations of V and D, does perform better in Case 2 than in Case 1. Furthermore, Vol outperforms $R_{\max}$ and $R_{\min}$ for the largest values of V/D in Case 2. These features of Vol are likely the result of Vol encoding aspects of junction behavior—particularly what we interpret as congestion at junctions—not captured by the other metrics (Sarhad et al. 2014).

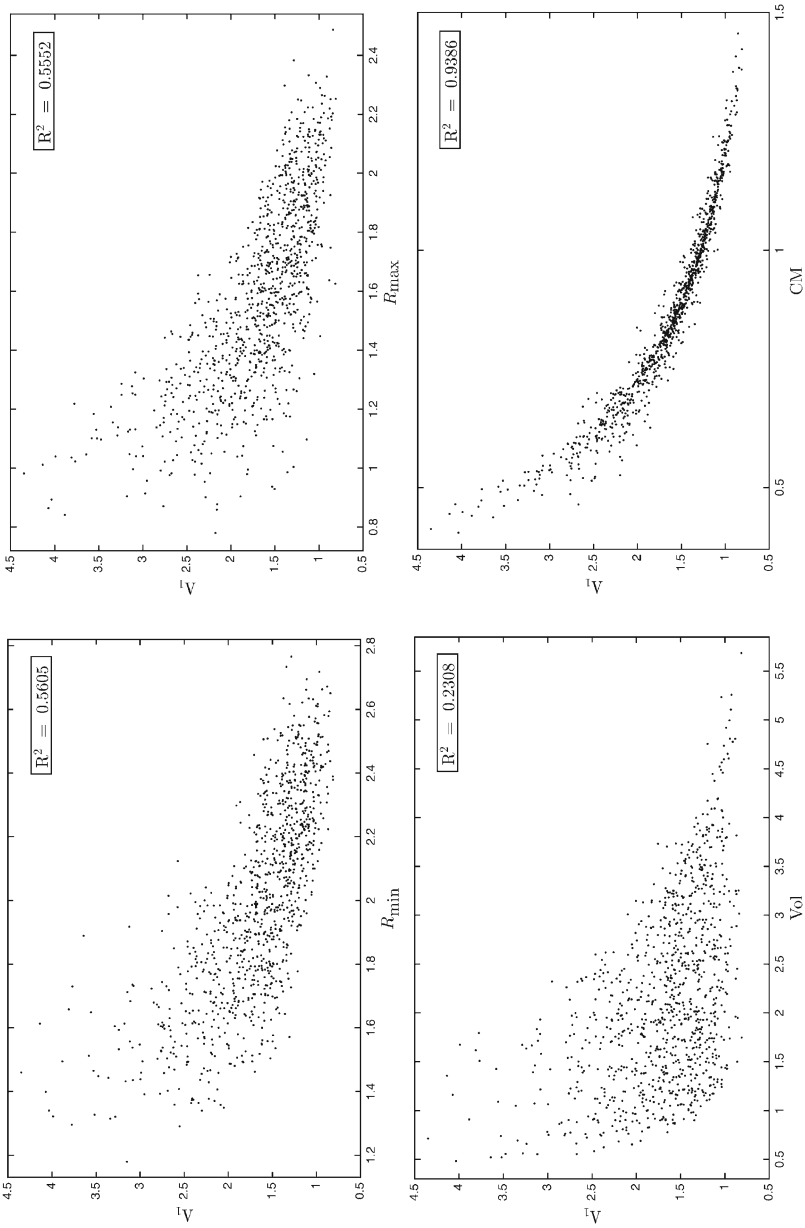

Fig. 5 Persistence metrics for Case 2. This figure is a duplication of Fig. 4 except that in the stochastic generation of the 1000 trees, the Case 1 area condition (2.11) is replaced by the Case 2 area condition (2.12). The dispersal parameters are again held constant at $V = D = 1$. CM's R^2 value holds close to its value in Case 1 and more drastically outperforms $R_{\max}$ and $R_{\min}$

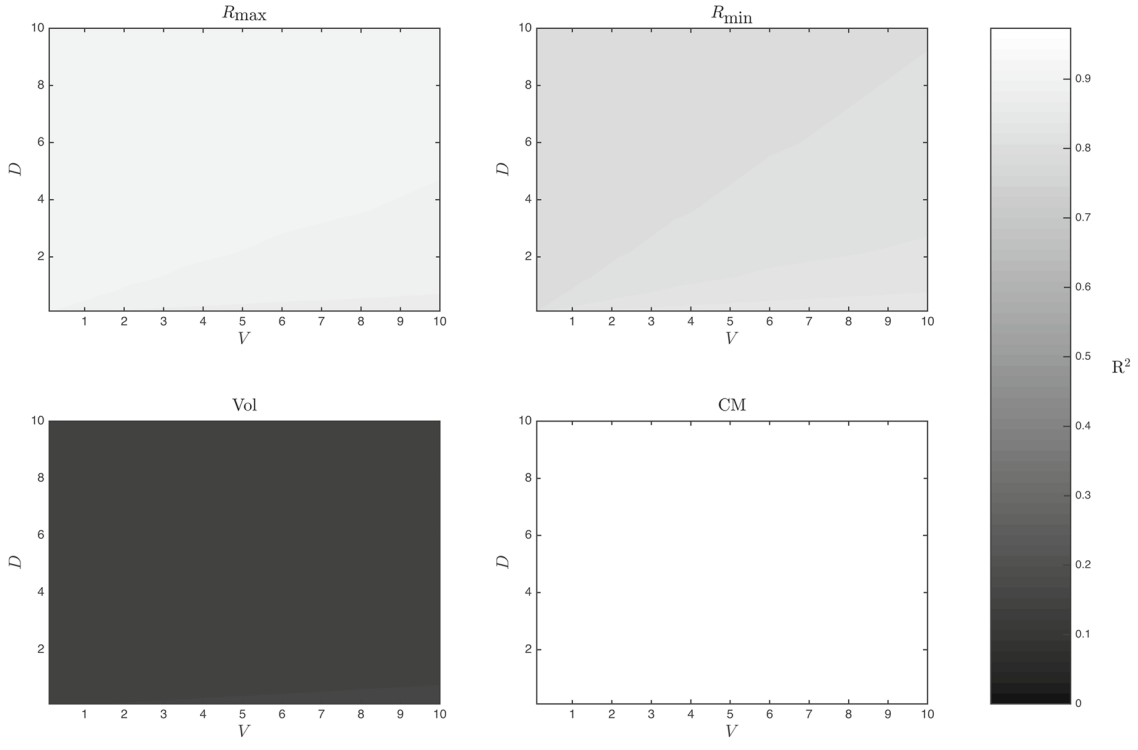

Fig. 6 Case 1: Performance of metrics under different diffusion and advection rates. One hundred networks are stochastically generated per Case 1 area conditions and principal eigenvalues are computed for each network. For each combination of V and D, a plot of eigenvalue versus metric is generated (as in Figs. 4, 5) and a corresponding R^2 value is computed. The *shading scale* summarizes the R^2 results for each metric across the range of V and D combinations (discretized in a 10×10 grid). Almost uniform shading at each V and D combination within each given metric demonstrates minimal differences in that metric's performance while strong differences in shading among metrics demonstrate equally strong differences in performance. CM maintains it superiority over the other metrics and is near $R^2 = 1$ over the entire range

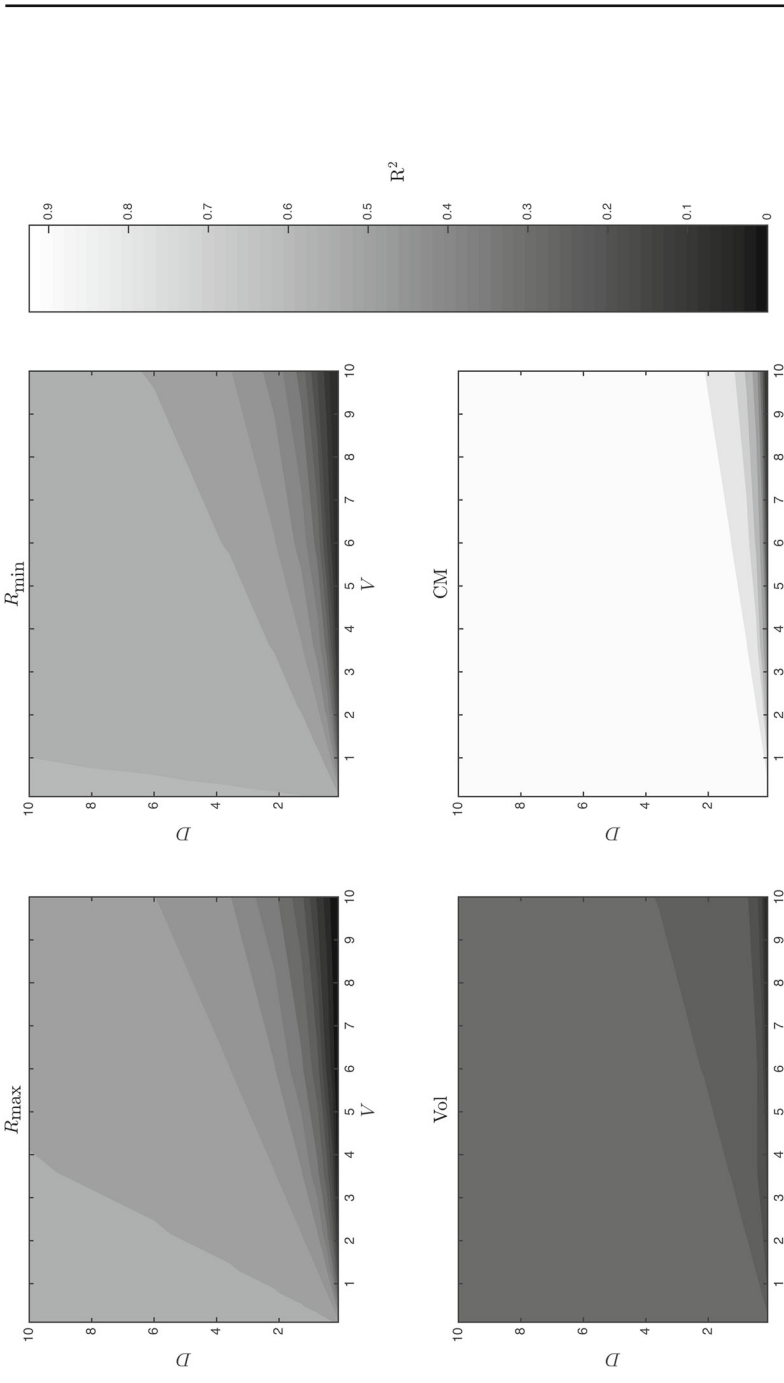

Fig. 7 Case 2: Performance of metrics under different diffusion and advection rates. Exactly as in Fig. 6, except the 100 networks are generated using Case 2 area conditions (2.12). CM suffers some breakdown as a persistence indicator in the range of the highest V values combined with the lowest D values, but features an R^2 value above 0.9 for all but a few combinations of V and D. All metrics suffer in this region and perform worse than in Case 1, with the exception of Vol which slightly improves in Case 2

The analyses presented thus far show that CM is the best predictor of Λ_1, and hence persistence, than the other metrics for the types of networks we consider here. Moreover, these results reinforce the intuition gained in Sarhad et al. (2014) regarding the importance of habitat distribution in the context of advection towards a lethal habitat boundary. Heuristically, a larger CM implies that more habitat, and hence more of the population, is distributed farther away from the lethal boundary, enhancing persistence. However, CM can suffer under Case 2 conditions when V is relatively large (Fig. 7). In Sects. 3.4 and 4, we examine CM further, both for its strength and weakness (i.e., the persistence-related information it can and cannot encode), proposing a reason for the weakness and an idea for shoring up the shortcoming.

3.4 Another look at CM

In this section we make the case that CM is a proper generalization of length in the finite segment model to the types of branching networks we consider here in the context of advection towards the lethal root. At the same time, we investigate the complications that Case 2 area conditions—combined with high advection—creates for CM as a persistence predictor. Also discussed is the possibility of augmenting CM with another metric to create a stronger proxy for Λ_1.

Our approach involves the eigenvalue-determining formula for the interval problem with zero flux (ZF) upstream and lethal downstream conditions (Speirs and Gurney 2001):

$$\sqrt{\frac{4D\Lambda - V^2}{4D^2}} = -\frac{V}{2D}\tan\left[L\sqrt{\frac{4D\Lambda - V^2}{4D^2}}\right] \tag{3.1}$$

To demonstrate the equivalence between CM and length in a single segment model, we simply substitute 2CM for length L in (3.1) and solve for the smallest positive root Λ_1. This value is then compared against values for Λ_1 from networks with Case 1 and 2 area conditions across a range of CM values (Fig. 8).

CM performs consistently well under Case 1 conditions. In Case 2, however, CM does somewhat underestimate persistence for networks at high V and large CM values. Interestingly, underestimation also occurs when V is small and CM is also small. The results in Fig. 8 provide compelling evidence that CM is a proper "system length" of networks examined here with advection towards a lethal root (see also Fig. 9). Yet, there is clearly a missing component of persistence which we speculate is due to junction behavior that is persistence enhancing when the sum of upstream areas is larger than the downstream branch and advection is high. This junction behavior would not be observed in an simple interval model and thus would be missing from *typical* "system length" or CM-type metrics.

4 Discussion

The many geometric parameters that define branching biological networks make it difficult to predict population persistence outcomes based on network geometry.

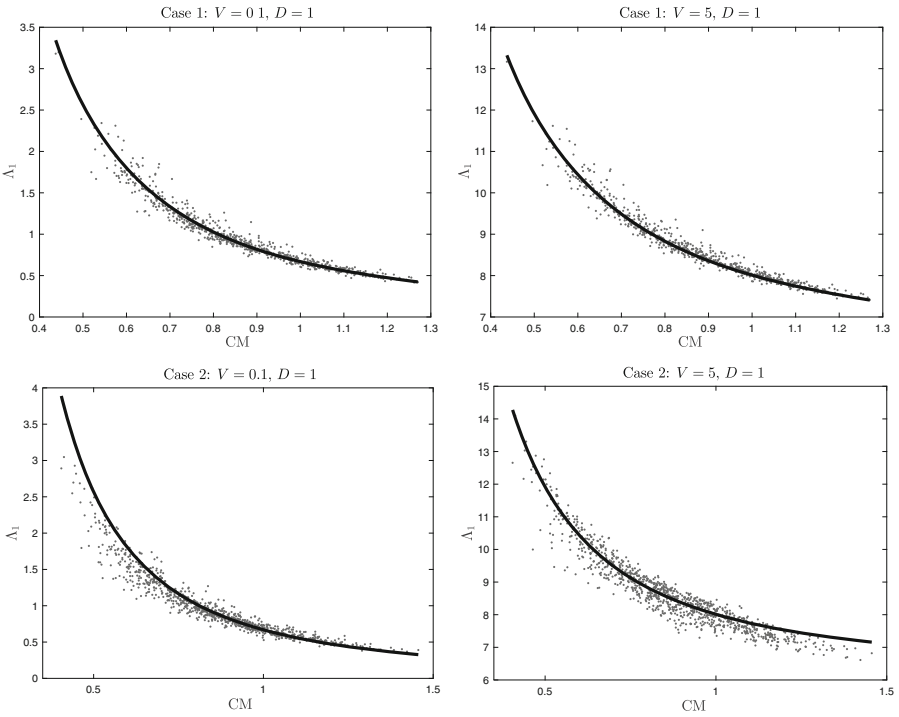

Fig. 8 CM as a system length. We substitute 2CM for L in (3.1) and solve for Λ_1, plotting a *continuous curve* (*bold*) against CM, which is then compared to the 1000-point CM versus Λ_1 point clouds (*gray circles*). Although (3.1) is "blind" to any network structure, CM serves as a strong proxy for length in (3.1) in Case 1. Some breakdown occurs in Case 2, particularly an underestimation of persistence when V and CM are both small and both large

This is especially the case for metric graphs that model spatially-continuous habitat on graph edges. Metric graphs that we employ here contain potential variation in edge lengths and area relations at junctions, making intuition illusive even for relatively small metric graph networks (e.g. Sarhad et al. 2014). Here, we sought to advance the application of metric graphs in biology by investigating how global geometric features of branching networks modeled as metric graphs characterize population persistence. The particular case study was of a population dispersing by diffusion and advection toward a lethal downstream boundary, which has received extensive previous attention (Speirs and Gurney 2001; Lutscher et al. 2005, 2007; Ramirez 2012; Sarhad et al. 2014; Sarhad and Anderson 2015). Towards this end, we examined various metrics related to network geometry and tested their robustness as indicators of population persistence in stochastically generated branching networks. Branching networks possessed stochastic variation in edge lengths and area conditions. Rules governing area conditions were broken into two cases, the second being more general, allowing our results to serve as a springboard for future work modeling a wide variety of different organisms and types of biological networks.

The metrics we examined encoded different aspects of network length and/or volume. One of these, the Center Metric (CM), far outperformed other metrics that focused solely on the total habitat volume of the network (Vol), the distance from the lethal boundary to the nearest upstream boundary ($R_{\min}$), and the distance from the lethal boundary to the farthest upstream boundary ($R_{\max}$). Inspired by previous work in river hydrology (e.g. Rodriguez-Iturbe and Rinaldo 2001) and metric graphs (e.g, Sarhad et al. 2014), CM in our context captures the distribution of habitat within in the network in a way that respects distance to the single lethal boundary at the network root. Moreover, our results provide evidence that CM performs well as an indicator of population persistence because it is an appropriate "system length" for branching networks, possessing a similar relationship with the dominant eigenvalue as segment length does in the single-segment population models (e.g. Speirs and Gurney 2001).

While our results suggest that CM is a promising indicator of persistence for the types of networks we examine in this article, it can underestimate persistence outcomes for some networks. This is particularly true in networks that feature Case 2 junction conditions and high advection speeds (Figs. 7, 8), as CM does not encode some important junction behavior. Junction conditions can strongly influence the principal eigenvalue and hence population persistence in metric graphs (see also Kostrykin and Schrader 2006; Berkolaiko and Kuchment 2012; Sarhad et al. 2014; Sarhad and Anderson 2015), yet it is unknown how to best characterize such effects. A single "system length", CM, is not enough to encode persistence behavior for indefinitely broad parameter ranges in the Case 2 setting. Instead, another metric that encodes junction behavior (as well as possibly an "average location" of this overall junction behavior) of the network is necessary to build a stronger predictor of persistence. We conjecture that such a metric—together with CM—could be used in a formula similar to (3.1) to become an excellent, yet simple, predictor of population persistence. A combined metric could also potentially yield tight upper and lower (statistical) bounds for persistence outcomes for some analytic bounds on principal eigenvalues for (2.2) (see Sarhad et al. 2014). Interestingly enough, just as CM does not completely ignore junction behavior, the desired junction behavior metric would not necessarily be blind to location and distance in the network.

The graphs we examine here are purposefully selected to be relatively simple in order to balance generality and tractability in the interpretation of results. While our algorithm is capable of generating a wide range of topologies and geometries, our generated networks still all belonged to a class of 14 vertex rooted trees that were binary save for the root vertex. In contrast, there is a large body of literature that examines a wide array of branching network structures and the variety of processes that can generate them (Rodriguez-Iturbe and Rinaldo 2001; Bentley et al. 2013; Zanardo et al. 2013). One focus of this literature is how area and volume distributions in the network change with underlying rules of construction (e.g. Rodriguez-Iturbe and Rinaldo 2001; Lashermes and Foufoula-Georgiou 2007). Ecological studies that have examined population persistence and dynamics in branching networks have tended to use simplified representations of network topology as we have done here, although the specific choices vary across studies, including radial (Fagan 2002; Goldberg et al.

2010; Sarhad et al. 2014; Sarhad and Anderson 2015) and non-radial binary trees (Carrara et al. 2012), non-binary trees (Yeakel et al. 2014), and topologies of actual river networks (Muneepeerakul et al. 2007). An important area of future research is to merge persistence studies with more system-specific topological and geometric studies. Understanding whether persistence outcomes change predictably given changes in algorithms used to generate the networks is an important step in applying our results to more realistic contexts. Additionally, such work is necessary to determine the generality of CM or related metrics as persistence predictors. However, given the wide range of available topologies and geometries, it is worth exploring standardized strategies for moving forward. One potential method would be to quantify deviations from radial networks (networks for which all geometric properties depend only on the distance from the root) and the subsequent deviations in persistence outcomes, as persistence calculations in radial networks are analytically more tractable and possess a minimum number of parameters for ease of interpretation (e.g., Sarhad et al. 2014; Sarhad and Anderson 2015). Studies could characterize how far the non-radial network principal eigenvalue is from a fixed radial network's eigenvalue, given the non-radial network's similarity (or "distance") from the radial network, and whether metrics like CM capture these deviations.

Beyond topology and geometry, the quantum graph framework employed here is flexible enough to be extended to include features known to be important in real biological and ecological networks. These could include additional spatial heterogeneity in vital and movement rates as well as the inclusion of species interactions (e.g., competition or predation). Previous single-segment models have found both within-segment spatial variation (Lutscher et al. 2006, 2007; Jin and Lewis 2011; Lam et al. 2016) and species interactions (Lutscher et al. 2007; Hilker and Lewis 2010) can dramatically alter persistence outcomes. These issues have not been explored as extensively in the framework of branching networks (but see Goldberg et al. 2010; Auerbach and Poff 2011). For metric graphs, Ramirez (2012) found that combinations of movement rates that guarantee persistence in sub-graphs extend persistence to the entire network, nullifying the effects of any global geometric structure. This latter result is particularly important in the context of this article, as it implies that variation in V and D may require consideration of a broader class of metrics. As the CM metric appears to work well in the absence of within-segment heterogeneity, it could also serve as a bound on persistence when V and D are variable and less predictable. Regardless, what is clear from our work and that of others is that exploration of persistence outcomes in these more complex situations in metric graphs does not lend itself to analytic solutions. For this reason, it is important to gain as much insight as possible for the simplest working models before venturing into more complex ones. That said, the ultimate goal for this line of research is to expand quantum graph theory to include realistic spatial and temporal heterogeneity so that system-specific models can be developed and tested against empirical data from actual biological systems.

Acknowledgements We would like to thank Robert Carlson, James Kelliher, Frithjof Lutscher, and Michael Neubert for insightful discussions on population persistence in river networks. We also thank two anonymous reviewers whose comments improved the manuscript.

5 Appendix

5.1 The eigenvalue problem and persistence criteria

Some manipulations of (2.5) simplify analysis so that the study of persistence can be reduced to studying the principal eigenfunction and eigenvalue of an associated second order differential equation without a first derivative term. The change of variables $U_e(x_e) = \exp[Vx_e/(2D)]g_e(x_e)$ eliminates the first derivative term. This change of variables combined with the substitution

$$D\phi = \Lambda - \frac{V^2}{4D} \tag{5.1}$$

yields the very simple (self-adjoint) Laplacian eigenvalue problem

$$\frac{\partial^2 g_e}{\partial x_e^2} + \phi g_e = 0 \tag{5.2}$$

defined edgewise on the network with boundary and junction conditions inherited from the RDA (2.2) (Sarhad et al. 2014). The advection V now only appears in the boundary and junction conditions and in the persistence criteria. If ϕ_1 denotes the principal eigenvalue of (5.2), then by (5.1), $\Lambda_1 = D\phi_1 + V^2/(4D)$ and solving for Λ_1 is reduced to solving for ϕ_1. In terms of the boundary and junction conditions, the lethal condition and the downstream boundary is unchanged for (5.2), while for the upstream boundary condition in (2.3) and junction condition in (2.7), $V/2$ is substituted for V.

In a single segment model, there are no junctions and simply the two boundary conditions. A general solution to the eigenvalue problem $g_e'' + \phi g_e = 0$ can be written in the form $g_e(x_e) = c_1 exp[ipx_e] + c_2[-ipx_e]$ where $p = \sqrt{\phi}$. Applying the two boundary conditions yields two equations and for the unknowns c_1 and c_2 which can subsequently be written in a matrix form $Z\hat{c} = 0$ where $\hat{c} = (c_1, c_2)$, and $Z = Z(\phi)$ is a 2×2 matrix with elements dependent on ϕ. A nontrivial solution for $\hat{c}$ is desired, which occurs if and only if $\det Z(\phi) = 0$. Now the discrete ϕ_k, and therefore Λ_k can be solved for (see (3.1)) (as can the countable eigenfunctions g_e^k). Given an initial population distribution, the time dependent solution of the original linearized RDA Eq. (2.2) can be written in terms of an infinite linear combination of these eigenfunctions, where $\lambda = r - \Lambda_1$ determines whether or not the solution grows, indicating persistence, or shrinks to zero, indicating extinction. This is routine analysis for a segment; for an example of the time dependent solution and persistence criteria in a segment or tree, see equation 2.21 and Theorem 1 in Sarhad et al. (2014).

The extension to trees is similar, except that each junction replaces a boundary condition for 3 incident segments, so that in a 3-edge tree graph for example, there are 3 boundary conditions while the junction condition provides an additional 3 conditions paired with the three general solutions $U_e\,(x_e) = c_{1e} \exp[ipx_e] + c_{2e} \exp[-ipx_e]$ on the 3 edges ($e = 0, 1, 2$). This leads to 6 equations and 6 unknowns c_{ae} ($a = 1, 2$), and a matrix equation $Z(\phi)\hat{c} = 0$, where $\hat{c} = (c_{ab})$. In general, if there are m edges,

this problem yields a $2m \times 2m$ system and Z is a $2m \times 2m$ matrix. Again, a nontrivial solution for $\widehat{c}$ is desired which occurs if and only if $\det Z(\phi) = 0$. See, for example, Kostrykin and Schrader (2006), pages 202–208 for a detailed recipe for constructing the matrix Z. For the readers' convenience, we provide a sample computation for a 3 edge network in Sect. 5.3.

At this point, it is worth discussing the mathematical requirements that ensure that our population model and subsequent principal eigenvalue of analysis of the linearized Eq. (2.2) are meaningful in the context of population persistence. In Sarhad et al. (2014), the constraint that $A_0V \geq A_1V + A_2V$ was proved sufficient (but not necessary) to ensure the validity of the persistence study. This constraint is satisfied by each vertex of Case 1 networks but may or may not be satisfied at each vertex of Case 2 networks.

The requirements for a valid analysis include that a population with $\lambda < 0$ goes to zero uniformly as $t \to \infty$, an initial positive population is nonnegative in time for $t > 0$, that the eigenspace of the principal eigenvalue Λ_1 has dimension one, that there exists a nonnegative principal eigenfunction that will not be orthogonal to any initial positive population, and that $\Lambda_1 > 0$. If this last requirement fails, in particular, a population could grow for a growth rate $r \leq 0$ which would be nonsensical for the processes modeled by the RDA equation. However, if $\Lambda_1 = r - \lambda > 0$, then necessarily $r > \lambda$. Given the persistence criteria which requires $\lambda > 0$, persistence requires $r > \lambda > 0$ and hence a population cannot grow if $r \leq 0$.

Numerical analysis in Sarhad et al. (2014), Sarhad and Anderson (2015) and in the current article strongly support the conjecture that $\Lambda_1 > 0$ also when $A_0V < A_1V + A_2V$, and therefore for all networks which arise in Case 2. Moreover, we conjecture, based on various numerical investigations of solutions, that $\Lambda_1 > 0$ is sufficient to ensure the other requirements and thus warrants the inclusion of the $A_0V < A_1V + A_2V$ condition. Additionally, extending Case 2 to allow for this condition increases the geometric variability of our networks in a manner that increases demands on our geometric indicators of persistence, since all of them, including CM, are blind to at least some aspect of junction behavior. Furthermore, all perform worse as predictors in Case 2. This last result supports our argument in the discussion that an appropriate network "size" or length must be augmented by another indicator which encodes junction behavior more directly.

5.2 Stochasticity in root values vs. CM

In our studies, root edge lengths and areas were chosen from [0.5, 1.5] and [0.5, 2], respectively. As all lengths and areas are scaled regularly (up to stochasticity) from their respective root values in our studies, we would not expect this variation to affect the robustness of geometric indicators. This is particularly true in the case of areas, where Λ_1 only depends on the ratios A_1/A_0 and A_2/A_0, and not on a uniform rescaling of areas [(2.7), (2.3); see Sarhad et al. 2014 for additional explanation].

However, to see examples of how a larger or smaller range of stochasticity in the root values affect the robustness of CM, we feature two studies under Case 1 conditions (parallel studies for Case 2 are not pictured since they offer no additional insight in

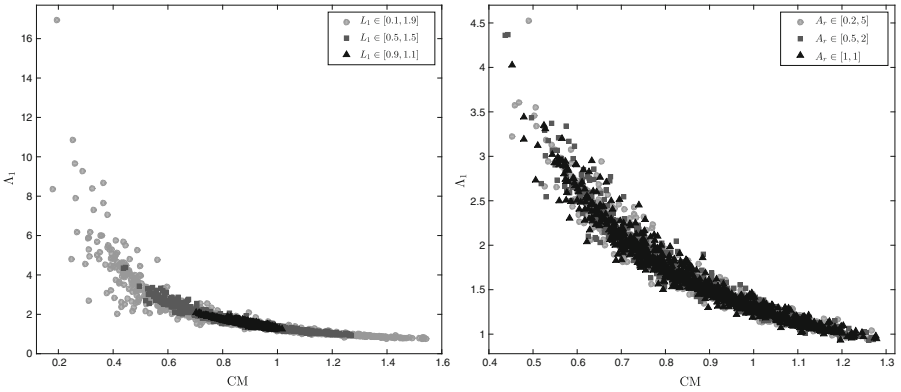

Fig. 9 Varying the root edge length and area distributions. Two additional sets of 1000 Case 1 trees are stochastically generated using smaller and larger root edge distributions. In all previous studies in the current article, root edge lengths and areas were chosen, respectively, from [0.5, 1.5] and [0.5, 2]. Here we look at CM's correlation with Λ_1 for smaller and larger distributions. CM's correlation with the original set of 1000 Case 1 trees is included for comparison. The dispersal parameters are set at $V = D = 1$

this context). Stochastic generation is as described in Sect. 2 and a different set of 1000 trees is generated from each of the two additional sets of root edge distributions used in Fig. 9. Advection and diffusion are held constant at 1 ($V = D = 1$). Figure 9 (left), for the largest distribution of root edge lengths, displays the effect of an increasing (and decreasing) CM on the eigenvalue. As the graph diameter increases and decreases, CM reflects movement proportional to an inverse square curve similar to what occurs with length in a single segment model, confirming intuition, and consistent with the case we have made for CM as a proper system length. As in previous studies in the paper with all metrics, there is some breakdown when the metric value is small. The broadest distribution used for root edge length, just as it allows for much longer networks (large CM), also allows for much shorter networks (small CM) and so in the smallest CM range of Fig. 9 (left), there is the most break down in correlation with Λ_1. Figure 9 (right) depicts the effect of changes to the root edge cross section to Λ_1, which can be interpreted as a uniform rescaling of the habitat in our system. Paralleling the interval model, Fig. 9 (right) shows no statistically significant effect from such habitat scaling, reflecting what is already known, that the model is sensitive only to local area scaling and invariant to a global rescaling (without stochasticity in network generation for the three simulations, the 3 data point clouds would coincide exactly, rather than nearly).

5.3 Principal eigenvalue for a star graph

In the following we provide an example principal eigenvalue computation for a three edge ("star") graph Γ. Let L_e and A_i ($e = 0, 1, 2$) denote the lengths and cross-sectional areas, respectively, of three edges, with the downstream edge indexed by $e = 0$ and the two upstream edges indexed by $e = 1$ and $e = 2$. Given the discussion in Sect. 5.1, in order to compute the principal eigenvalue Λ_1 corresponding to (2.5) in Sect. 2, we can first find the eigenvalue ϕ_1 corresponding to the eigenvalue Eq. (5.2) presented in Sect. 5.1:

$$\frac{\partial^2 g_e}{\partial x_e^2} + \phi g_e = 0$$

Here, g_e is the restriction of the eigenfunction to an edge e and the eigenfunction (a 3-vector whose elements are functions) is $\overline{g} = \left(\{g_e\}_{e=0,1,2}\right) = (g_0, g_1, g_2)$. While (2.5) is subject to the zero flux and continuity condition C ((2.7) and (2.8)) at the lone junction of Γ, the lethal condition (2.3) at the root (the downstream most vertex; the terminal end of e_0) and the zero flux condition ZF (2.3) at the upstream most boundaries (the terminal ends of e_1 and e_2), the eigenvalue equation above (5.2) is subject to the exact same conditions except the advection V is replaced by $V/2$ (due to the substitution eliminating the first derivative term; see the discussion in Sect. 5.1).

In terms of the junction condition C which, in general, includes the eigenfunction and its first derivative, it is often convenient to parametrize the functions so that the junction is located at 0 and the derivatives are computed in the direction outward of the junction. In light of this, the zero flux condition C which says that "the population flux into a junction equals the population flux out of a junction" is recast in the equivalent statement, "the sum of the outward population fluxes at a junction is equal to zero." Recalling that a downstream parametrization is described in Sect. 2 and that a change in the direction of the parametrization of the two upstream incident edges is equivalent to changing the sign of the derivatives of the upstream edge functions, the change, symbolically, is as follows:

$$A_0\left(\frac{V}{2}g - D\frac{\partial g_0}{\partial x_0}\right)(0) = A_1\left(\frac{V}{2}g - D\frac{\partial g_1}{\partial x_1}\right)(0) + A_2\left(\frac{V}{2}g - D\frac{\partial g_2}{\partial x_2}\right)(0)$$

becomes

$$A_0\left(\frac{V}{2}g - D\frac{\partial g_0}{\partial x_0}\right)(0) = A_1\left(\frac{V}{2}g + D\frac{\partial g_1}{\partial x_1}\right)(0) + A_2\left(\frac{V}{2}g + D\frac{\partial g_2}{\partial x_2}\right)(0)$$

It useful to recall that the reason there is no subscript on $g(0)$ is because condition C imposes continuity at the junction so that $g(0)$ can replace $g_0(0) = g_1(0) = g_2(0)$. To simplify the notation we will use "prime" notation for the spatial derivatives and use sigma notation for summing. Rearranging terms, the junction condition for (5.2) is written compactly as

$$\sum_{e=0}^{2} A_e g_e'(0) = \left[(A_0 - A_1 - A_2)\frac{V}{2D}\right] g(0) \tag{5.3}$$

Maintaining the convention that derivatives are computed in the direction outward of the junction 0, we can write the boundary conditions for (5.2) as

$$\underbrace{g_0(0) = 0}_{\text{lethal root}} \qquad \underbrace{g_1'(L_1) = -\frac{V}{2D}g_1(L_1) \qquad g_2'(L_2) = -\frac{V}{2D}g_2(L_2)}_{\text{zero flux at upstream boundaries}} \tag{5.4}$$

As one can verify by inspection, the junction and boundary conditions imposed on $\overline{g}$ and $\overline{g}'$, (5.3) and (5.4), are easily expressed in (6×6) matrix form (Kostrykin and Schrader 2006):

$$\underbrace{\begin{pmatrix} 1 & -1 & 0 & 0 & 0 & 0 \\ 0 & 1 & -1 & 0 & 0 & 0 \\ 0 & 0 & F & 0 & 0 & 0 \\ 0 & 0 & 0 & 1 & 0 & 0 \\ 0 & 0 & 0 & 1 & G & 0 \\ 0 & 0 & 0 & 0 & 0 & G \end{pmatrix}}_{A} \underbrace{\begin{pmatrix} g_0(0) \\ g_1(0) \\ g_2(0) \\ g_0(L_0) \\ g_1(L_1) \\ g_2(L_2) \end{pmatrix}}_{\overline{g}} + \underbrace{\begin{pmatrix} 0 & 0 & 0 & 0 & 0 & 0 \\ 0 & 0 & 0 & 0 & 0 & 0 \\ A_0 & A_1 & A_2 & 0 & 0 & 0 \\ 0 & 0 & 0 & 0 & 0 & 0 \\ 0 & 0 & 0 & 0 & 1 & 0 \\ 0 & 0 & 0 & 0 & 0 & 1 \end{pmatrix}}_{B} \underbrace{\begin{pmatrix} g_0'(0) \\ g_1'(0) \\ g_2'(0) \\ -g_0'(L_0) \\ -g_1'(L_1) \\ -g_2'(L_2) \end{pmatrix}}_{\overline{g}'} = \underbrace{\begin{pmatrix} 0 \\ 0 \\ 0 \\ 0 \\ 0 \\ 0 \end{pmatrix}}_{\overline{0}}$$

where

$$F = -(A_0 - A_1 - A_2)\frac{V}{2D} \qquad G = -\frac{V}{2D}$$

(This is, of course, not the only way to represent the junction and boundary conditions using matrix arithmetic, and in particular, the matrices A and B can be arranged differently; this particular form uses a convenient basis for the problem.) The restriction of $\overline{g}$ to each edge $e = 0, 1, 2$ must be of the form

$$g_e(x_e) = c_{1e} \exp[ipx_e] + c_{2e} \exp[-ipx_e]$$

where $i = \sqrt{-1}$ and $p = \sqrt{\phi}$. Then

$$g_e'(x_e) = ipc_{1e} \exp[ipx_e] - ipc_{2e} \exp[-ipx_e]$$

for each edge e. Computing these derivatives outward of the junction 0, and imposing the junction and boundary conditions at 0, L_0, L_1, and L_2 on $\overline{g}$ and $\overline{g}'$, $\overline{g}$ is an eigenfunction of (5.2) with eigenvalue ϕ if and only if it satisfies the following homogeneous matrix Equation (Kostrykin and Schrader 2006):

$$Z \begin{pmatrix} c_{10} \\ c_{11} \\ c_{12} \\ c_{20} \\ c_{21} \\ c_{22} \end{pmatrix} = \overline{0} \tag{5.5}$$

where Z is the 6×6 matrix given by

$$Z = AX + ipBY$$

and X and Y are the 6×6 matrices given by

$$\underbrace{\begin{pmatrix} 1 & 0 & 0 & 1 & 0 & 0 \\ 0 & 1 & 0 & 0 & 1 & 0 \\ 0 & 0 & 1 & 0 & 0 & 1 \\ e^{ipL_0} & 0 & 0 & e^{-ipL_0} & 0 & 0 \\ 0 & e^{ipL_1} & 0 & 0 & e^{-ipL_1} & 0 \\ 0 & 0 & e^{ipL_2} & 0 & 0 & e^{-ipL_2} \end{pmatrix}}_{X}$$

$$\underbrace{\begin{pmatrix} 1 & 0 & 0 & -1 & 0 & 0 \\ 0 & 1 & 0 & 0 & -1 & 0 \\ 0 & 0 & 1 & 0 & 0 & -1 \\ -e^{ipL_0} & 0 & 0 & e^{-ipL_0} & 0 & 0 \\ 0 & -e^{ipL_1} & 0 & 0 & e^{-ipL_1} & 0 \\ 0 & 0 & -e^{ipL_2} & 0 & 0 & e^{-ipL_2} \end{pmatrix}}_{Y}$$

If the L_e and A_e, $e = 0, 1, 2$, are given, then Z is a function of ϕ only and the homogeneous matrix Eq. (5.5) has a nontrivial solution (the c_{ae} for $a = 1, 2$ and $e = 0, 1, 2$ must not all be equal to zero) if and only if ϕ satisfies

$$\det Z(\phi) = 0 \tag{5.6}$$

Since the eigenvalues of (5.2) are real numbers and strictly bounded below by 0 for Case 1 (and some Case 2) area conditions (Sarhad et al. 2014), there is a smallest positive $\phi = \phi_1$ which satisfies (5.6). For the general Case 2 condition, it is conjectured and supported by numerical evidence, that the eigenvalues of (5.2) are strictly bounded below by $-V^2/4D$, so that there is a smallest eigenvalue $\phi = \phi_1 > -V^2/4D$. In either case, once the eigenvalue ϕ_1 is computed (e.g., with the aid of a root finder in programs like MATLAB or Mathematica), the principal eigenvalue Λ_1 for (2.5) is computed using (5.1) from Sect. 5.1, and so

$$\Lambda_1 = D\phi + \frac{V^2}{4D}$$

The following is a sample computation for $A_0 = 1$, $A_1 = 1/2$, $A_2 = 1/2$, and $L_e = 1$ for $e = 0, 1, 2$ (which reduces to a single segment model of length 2; see Sarhad et al. (2014) which shows a radial tree with the Case 1 condition reduces to the single segment model with zero flux upstream boundary condition and lethal root boundary condition). In this case, Z becomes

$$\underbrace{\begin{pmatrix} 1 & -1 & 0 & 1 & -1 & 0 \\ ip & \frac{ip}{2} & \frac{ip}{2} & -ip & -\frac{ip}{2} & -\frac{ip}{2} \\ 0 & 0 & 1 & 0 & 0 & -1 \\ e^{ip} & 0 & 0 & e^{-ip} & 0 & 0 \\ 0 & -\frac{1}{2}e^{ip} - ie^{ip}p & 0 & 0 & -\frac{1}{2}e^{ip} + ie^{ip}p & 0 \\ 0 & 0 & -\frac{1}{2}e^{ip} - ie^{ip}p & 0 & 0 & -\frac{1}{2}e^{ip} + ie^{ip} \end{pmatrix}}_{Z}$$

while the determinant of Z is given by

$$\begin{aligned} \det Z(\phi) = \frac{1}{2}e^{-3ip}p(i - ie^{6ip}(i-2p)^2 + 4p - 4ip^2 \\ - ie^{2ip}(1+4p^2) - ie^{4ip}(1+4p^2)) \end{aligned}$$

Recalling that $p = \sqrt{\phi}$ and solving $\det Z(\phi) = 0$ for the smallest solution (ϕ_1), yields $\phi_1 \approx 1.029$ so that $\Lambda_1 \approx 1.029 + 0.250 = 1.279$. Note that this is the answer you get from the single segment eigenvalue determining Eq. (3.1).

For an extreme Case 2 example, where $A_0 \ll A_1 + A_2$, ϕ can be very close to the conjectured lower bound: Let $A_1 = 1$, $A_2 = 1000$, $A_3 = 500$, and $L_e = 1$ for $e = 0, 1, 2$. Then computing as above yields $\phi_1 \approx -0.248$ (note that this is very close to the conjectured lower bound on ϕ_1, $-V^2/4D = 0.250$), and therefore a principal eigenvalue $\Lambda_1 \approx .002$ (which is positive and maintains that the intrinsic (linearized) growth rate r must be greater than 0 to ensure persistence, i.e. to ensure $\lambda = r - \Lambda_1 > 0$).

Finally, we note that a star graph is a very simple tree graph and it is easy to find a nice addressing system for the edges and subsequently a convenient basis for the matrix problem. For the more general (and larger) tree graphs generated in the current article, we refer the reader to Kostrykin and Schrader (2006).

References

Albert R, Barabasi AL (2002) Statistical mechanics of complex networks. Rev Mod Phys 74:47–97

Altermatt F (2013) Diversity in riverine metacommunities: a network perspective. Aquat Ecol 47:365–377

Anderson KE, Nisbet RM, Diehl S, Cooper SD (2005) Scaling population responses to spatial environmental variability in advection-dominated systems. Ecol Lett 8:933–943

Anderson KE, Paul AJ, McCauley E, Jackson LJ, Post JR, Nisbet RM (2006) Instream flow needs in streams and rivers: the importance of understanding ecological dynamics. Front Ecol Environ 4:309–318

Auerbach DA, Poff NL (2011) Spatiotemporal controls of simulated metacommunity dynamics in dendritic networks. J N Am Benthol Soc 30:235–251

Barrat A, Barthelemy M, Vespignani A (2008) Dynamical processes on complex networks. Cambridge University Press, New York

Bentley LP, Stegen JC, Savage VM, Smith DD, von Allmen EI, Sperry JS, Reich PB, Enquist BJ (2013) An empirical assessment of tree branching networks and implications for plant allometric scaling models. Ecol Lett 16:1069–1078

Berkolaiko G, Kuchment P (2012) Introduction to quantum graphs: mathematical surveys and monographs, vol 186. AMS, Providence

Brown BL, Swan CM, Auerbach DA, Grant EHC, Hitt NP, Maloney KO, Patrick C (2011) Metacommunity theory as a multispecies, multiscale framework for studying the influence of river network structure on riverine communities and ecosystems. J N Am Benthol Soc 30:310–327

Cantrell RS, Cosner C (2003) Spatial ecology via reaction–diffusion equations. Wiley, New York
Carrara F, Altermatt F, Rodriguez-Iturbe I, Rinaldo A (2012) Dendritic connectivity controls biodiversity patterns in experimental metacommunities. Proc Natl Acad Sci USA 109:5761–5766
Fagan WF (2002) Connectivity, fragmentation, and extinction risk in dendritic metapopulations. Ecology 83:3243–3249
Fausch KD, Torgersen CE, Baxter CV, Li HW (2002) Landscapes to riverscapes: bridging the gap between research and conservation of stream fishes. BioScience 52:483–498
Goldberg EE, Lynch HJ, Neubert MG, Fagan WF (2010) Effects of branching spatial structure and life history on the asymptotic growth rate of a population. Theor Ecol 3:137–152
Grant EHC, Lowe WH, Fagan WF (2007) Living in the branches: population dynamics and ecological processes in dendritic networks. Ecol Lett 10:165–175
Hilker FM, Lewis MA (2010) Predator–prey systems in streams and rivers. Theor Ecol 3:175–193
Jin Y, Lewis MA (2011) Seasonal influences on population spread and persistence in streams: critical domain size. SIAM J Appl Math 71(4):1241–1262
Kostrykin V, Schrader R (2006) Laplacians on metric graphs. In: Quantum graphs and their applications. Contemporary Mathematics, vol 415. AMS, pp 65–80
Lam K-Y, Lou Y, Lutscher F (2016) The emergence of range limits in advective environments. SIAM J Appl Math 76:641–662
Lashermes B, Foufoula-Georgiou E (2007) Area and width functions of river networks: new results on multifractal properties. Water Resour Res 43:W09405
Lutscher F, Pachepsky E, Lewis MA (2005) The effect of dispersal patterns on stream populations. SIAM J Appl Math 65:1305–1327
Lutscher F, Lewis MA, McCauley E (2006) Effects of heterogeneity on spread and persistence in rivers. Bull Math Biol 68:2129–2160
Lutscher F, McCauley E, Lewis MA (2007) Spatial patterns and coexistence mechanisms in systems with unidirectional flow. Theor Popul Biol 71:267–277
Muneepeerakul R, Weitz JS, Levin SA, Rinaldo A, Rodriguez-Iturbe I (2007) A neutral metapopulation model of biodiversity in river networks. J Theor Biol 245:351–363
Peterson EE, Hoef JMV (2010) A mixed-model moving-average approach to geostatistical modeling in stream networks. Ecology 91:644–651
Peterson EE, Ver Hoef JM, Isaak DJ, Falke JA, Fortin MJ, Jordan CE, McNyset K et al (2013) Modelling dendritic ecological networks in space: an integrated network perspective. Ecol Lett 16:707–719
Ramirez JM (2012) Population persistence under advection–diffusion in river networks. J Math Biol 65:919–942
Reynolds PG, Cuddington K (2012) Effects of plant gross morphology on predator consumption rates. Environ Entomol 41:508–515
Rodriguez-Iturbe I, Rinaldo A (2001) Fractal river basins: chance and self-organization. Cambridge University Press, Cambridge
Sarhad J, Anderson KE (2015) Modeling population persistence in continuous aquatic networks using metric graphs. Fundam Appl Limnol 186(1–2):135–152
Sarhad J, Carlson R, Anderson KE (2014) Population persistence in river networks. J Math Biol 69(2):401–448
Speirs DC, Gurney WSC (2001) Population persistence in rivers and estuaries. Ecology 82:1219–1237
Strogatz SH (2001) Exploring complex networks. Nature 410:268–276
Yeakel JD, Moore JW, Guimarães PR Jr, de Aguiar MAM (2014) Synchronisation and stability in river metapopulation networks. Ecol Lett 17:273–283
Zanardo S, Zaliapin I, Foufoula-Georgiou E (2013) Are American rivers Tokunaga self-similar? New results on fluvial network topology and its climatic dependence. J Geophys Res Earth Surf 118:2169–9011